Coupled K-matrix description of the reactions $\pi N \to \pi N$, $\pi N \to \eta N$, $\gamma N \to \pi N$, and $\gamma N \to \eta N$

A. M. Green[1,*] and S. Wycech[2,†]

[1]*Department of Physics and Helsinki Institute of Physics, P.O. Box 9, FIN-00014 University of Helsinki, Finland*
[2]*Soltan Institute for Nuclear Studies, Warsaw, Poland*

The coupled πN, ηN, γN systems are described by a K-matrix method. The parameters in this model are adjusted to get an optimal fit to $\pi N \to \pi N$, $\pi N \to \eta N$, $\gamma N \to \pi N$, and $\gamma N \to \eta N$ data in an energy range of about 100 MeV each side of the η threshold. The coupling of photons to the $N(1535)$ state is extracted and also an alternative to the current $S11 \gamma N \to \pi N$ amplitudes suggested. Expansions are given for the $\eta\eta$ and $\gamma\eta$ amplitudes in terms of the η momentum. Effects of interference of this state with background potential interactions are discussed and experimental consequences are indicated. [S0556-2813(99)00309-X]

PACS number(s): 13.75.−n, 25.80.−e, 25.40.Ve

I. INTRODUCTION

There is an increasing interest in η-meson physics both experimentally and theoretically. On the experimental side several facilities are now able to produce sufficient η's to enable a study to be made of their interactions with other particles. In particular, the photon machines MAMI [1] and GRAAL [2] are supplementing the earlier hadronic machines such as SATURNE [3], CELSIUS [4], and COSY [5]. The current theoretical interest stems partly from the early indications that the $\eta - N$ interaction is attractive and so could possibly lead to η-nucleus quasibound states (e.g., Refs. [6,7]). The theoretical approaches fall into two main categories. In the one, the various processes involving η-meson interactions are described in terms of microscopic models containing baryon resonances and the exchange of different mesons (e.g., Refs. [8,9]) which may be based on a chiral perturbation approach (e.g., Ref. [10]) or a quark model (e.g., Ref. [11]). Unfortunately, this approach requires a knowledge of the magnitudes and relative phases of many hadron-hadron couplings several of which are very poorly known. In addition, since η interactions — in the absence of η-meson beams — can only be studied as final-state interactions, one has to exploit relationships between the many processes involved. For example, in the present paper, the main interest is in the reaction (a) $\gamma N \to \eta N$. However, this is dependent on the final-state interaction (b) $\eta N \to \eta N$, which in turn depends on the reactions (c) $\pi N \to \eta N$ and (d) $\pi N \to \pi N$. Similarly, reactions (c) and (d) are related to (e) $\gamma N \to \pi N$. Therefore, any model that claims to describe reaction (a) must also see its implications in reactions (b), ... (e). This, we believe, is too ambitious a program at present. At this stage it is probably more informative to check the consistency between the data of the above five reactions and be able to relate them in terms of a few phenomenological parameters. When this has been accomplished, it will hopefully be possible to understand these parameters in terms of more microscopic models. With this in mind, in Ref. [12] a K-matrix model was developed by the authors to describe the reactions (a), (b), (c), and (d) in an energy range of about 100 MeV each side of the η threshold. This model was expressed in the form of two coupled channels for s-wave $\pi - N$ and $\eta - N$ scattering with the effect of the two-pion channel ($\pi N \to \pi \pi N$) being included only implicitly. The latter was achieved by first introducing the two-pion process as a third channel in the K matrix and subsequently eliminating that channel as an ''optical potential'' correction to the other two channels. It should be emphasized that this is not an approximation but is done only for convenience, since we do not address cross sections involving explicitly two final-state pions.

In Ref. [12] the η-photoproduction cross section was assumed to be proportional to the elastic $\eta - N$ cross section ($|T_{\eta\eta}|^2$). This is in line with the so-called Watson approximation [13]. In this way each of the matrix elements in the two-by-two T matrix of Ref. [12] was associated with some specific experimental data — $T_{\pi\pi}$ with the πN amplitudes of Arndt *et al.* [14], $T_{\pi\eta}$ with the η-production cross section in the review by Nefkens [15] and $T_{\eta\eta}$ with the η-photoproduction cross section of Krusche *et al.* [1].

In this paper we now wish to treat the γN channel explicitly. An enlargement of the K-matrix basis then permits a direct estimate of the matrix element $T_{\gamma\eta}$, so that $\sigma(\gamma N \to \eta N) \propto |T_{\gamma\eta}|^2$, thereby avoiding the earlier assumption that $\sigma(\gamma N \to \eta N) \propto |T_{\eta\eta}|^2$. The K matrix would now be a four-by-four matrix with the channels πN, ηN, $\pi \pi N$ and γN. In principle, ten different processes, corresponding to each matrix element, could be analyzed simultaneously. However, in practice, it is more convenient to elimate some channels by the ''optical potential'' method used already in Ref. [12]. We, therefore, describe in Sec. II the above reactions in terms of three separate T matrices. In Sec. III, we give the fitting strategy and also the numerical results in terms of the 13 parameters needed to specify the K matrices. This section also includes expansions — in terms of the η momentum — for the amplitudes of the $\eta N \to \eta N$ and $\gamma N \to \eta N$ reactions near the η threshold. Section IV contains a discussion and some conclusions.

II. THE K-MATRIX FORMALISM

In principle, the four channels of interest — πN, ηN, $\pi \pi N$ and γN — should be treated simultaneously. How-

*Electronic address: anthony.green@helsinki.fi
†Electronic address: wycech@fuw.edu.pl

ever, it is more convenient and transparent if the problem is analyzed in terms of three separate T matrices.

A. Coupled πN and ηN channels

The first T matrix is precisely the same as in Ref. [12], where only the πN and ηN channels — denoted by the indices π, η — are explicit. This can be written as

$$
T_1 = \begin{pmatrix} T_{\pi\pi} & T_{\pi\eta} \\ T_{\eta\pi} & T_{\eta\eta} \end{pmatrix} = \begin{pmatrix} \dfrac{A_{\pi\pi}}{1-iq_\pi A_{\pi\pi}} & \dfrac{A_{\pi\eta}}{1-iq_\eta A_{\eta\eta}} \\ \dfrac{A_{\eta\pi}}{1-iq_\eta A_{\eta\eta}} & \dfrac{A_{\eta\eta}}{1-iq_\eta A_{\eta\eta}} \end{pmatrix},
$$
(1)

where $q_{\pi,\eta}$ are the center-of-mass momenta of the two mesons in the two channels π, η and the channel scattering lengths A_{ij} are expressed in terms of the K-matrix elements, via the solution of $T=K+iKqT$, as

$$
A_{\pi\pi} = K_{\pi\pi} + iK_{\pi\eta}^2 q_\eta/(1-iq_\eta K_{\eta\eta}),
$$

$$
A_{\eta\pi} = A_{\pi\eta} = K_{\eta\pi}/(1-iq_\pi K_{\pi\pi}),
$$

$$
A_{\eta\eta} = K_{\eta\eta} + iK_{\eta\pi}^2 q_\pi/(1-iq_\pi K_{\pi\pi}).
$$
(2)

At this stage the $\pi\pi N$ channel is incorporated as an ''optical model'' correction to the corresponding matrix element of T_1 and the γN channel is simply ignored since this T matrix is used to describe only reactions (b), (c), and (d), where the effect of the γN channel is small being only an electromagnetic correction to these three reactions. As discussed in Ref. [12] various features of the experimental data suggest that the K-matrix elements can be parametrized in terms of energy independent constants — the background terms B_{ij} — plus poles associated with the S-wave πN resonances $N(1535)$ and $N(1650)$. This results in

$$
K_{\pi\pi} \to K_{\pi\pi}(a) = \frac{\gamma_\pi(0)}{E_0-E} + \frac{\gamma_\pi(1)}{E_1-E} + i\frac{K_{\pi 3}q_3 K_{3\pi}}{1-iq_3 K_{33}},
$$

$$
K_{\pi\eta} \to B_{\pi\eta} + \frac{\sqrt{\gamma_\pi(0)\gamma_\eta(0)}}{E_0-E} + i\frac{K_{\pi 3}q_3 K_{3\eta}}{1-iq_3 K_{33}},
$$

$$
K_{\eta\eta} \to K_{\eta\eta}(a) = B_{\eta\eta} + \frac{\gamma_\eta(0)}{E_0-E} + i\frac{K_{\eta 3}q_3 K_{3\eta}}{1-iq_3 K_{33}},
$$
(3)

where

$$
K_{33} = \frac{\gamma_3(0)}{E_0-E} + \frac{\gamma_3(1)}{E_1-E}, \quad K_{\pi 3} = \frac{\sqrt{\gamma_\pi(0)\gamma_3(0)}}{E_0-E}
$$

$$
+ \frac{\sqrt{\gamma_\pi(1)\gamma_3(1)}}{E_1-E}, \quad K_{\eta 3} = \frac{\sqrt{\gamma_\eta(0)\gamma_3(0)}}{E_0-E}.
$$

The last terms on the right-hand side (rhs) of Eqs. (3) represent the effect of the eliminated $\pi\pi N$ channel.

B. Coupled ηN and γN channels

The second T matrix involves only the two channels ηN and γN — denoted by the indices η, γ — where now it is the $\pi\pi N$ and πN channels that are treated as optical potentials. This T matrix is written as

$$
T_2 = \begin{pmatrix} T_{\eta\eta} & T_{\gamma\eta} \\ T_{\eta\gamma} & T_{\gamma\gamma} \end{pmatrix} = \begin{pmatrix} \dfrac{A_{\eta\eta}}{1-iq_\eta A_{\eta\eta}} & \dfrac{A_{\gamma\eta}}{1-iq_\eta A_{\eta\eta}} \\ \dfrac{A_{\eta\gamma}}{1-iq_\eta A_{\eta\eta}} & T_{\gamma\gamma} \end{pmatrix},
$$
(4)

where

$$
A_{\gamma\eta} = A_{\eta\gamma} = K_{\gamma\eta}/(1-iq_\gamma K_{\gamma\gamma}),
$$

$$
A_{\eta\eta} = K_{\eta\eta} + iK_{\gamma\eta}^2 q_\gamma/(1-iq_\gamma K_{\gamma\gamma}).
$$

Here we are not interested in $T_{\gamma\gamma}$, since this would describe the $\gamma N \to \gamma N$ reaction. The forms of $K_{\pi\pi}(a)$, $K_{\pi\eta}$, K_{33}, $K_{\pi 3}$, and $K_{\eta 3}$ are the same as given above. However,

$$
K_{\eta\eta} \to K_{\eta\eta}(b) = K_{\eta\eta}(a) + i\frac{K_{\eta\pi}q_\pi K_{\pi\eta}}{1-iq_\pi K_{\pi\pi}(a)}.
$$
(5)

Also, we now need

$$
K_{\gamma\eta} = B_{\gamma\eta} + \frac{\sqrt{\gamma_\gamma(0)\gamma_\eta(0)}}{E_0-E} + i\frac{K_{\gamma\pi}q_\pi K_{\pi\eta}}{1-iq_\pi K_{\pi\pi}(a)}
$$

$$
+ i\frac{K_{\gamma 3}q_3 K_{3\eta}}{1-iq_3 K_{33}},
$$
(6)

$$
K_{\gamma\gamma} = \frac{\gamma_\gamma(0)}{E_0-E} + \frac{\gamma_\gamma(1)}{E_1-E} + i\frac{K_{\gamma\pi}q_\pi K_{\pi\gamma}}{1-iq_\pi K_{\pi\pi}(a)} + i\frac{K_{\gamma 3}q_3 K_{3\gamma}}{1-iq_3 K_{33}},
$$
(7)

and

$$
K_{\gamma\pi} = B_{\gamma\pi} + \frac{\sqrt{\gamma_\gamma(0)\gamma_\pi(0)}}{E_0-E} + \frac{\sqrt{\gamma_\gamma(1)\gamma_\pi(1)}}{E_1-E} + i\frac{K_{\gamma 3}q_3 K_{3\pi}}{1-iq_3 K_{33}},
$$
(8)

where the last terms on the rhs represent the effect of the eliminated πN and $\pi\pi N$ channels. Also we need

$$
K_{\gamma 3} = \frac{\sqrt{\gamma_\gamma(0)\gamma_3(0)}}{E_0-E} + \frac{\sqrt{\gamma_\gamma(1)\gamma_3(1)}}{E_1-E}.
$$
(9)

C. Coupled πN and γN channels

The third T matrix involves only the two channels πN and γN — denoted by the indices π, γ — where now it is the ηN and $\pi\pi N$ channels that are treated as optical potentials. This T matrix is written as

$$T_3 = \begin{pmatrix} T_{\pi\pi} & T_{\gamma\pi} \\ T_{\pi\gamma} & T_{\gamma\gamma} \end{pmatrix} = \begin{pmatrix} \dfrac{A_{\pi\pi}}{1-iq_\pi A_{\pi\pi}} & \dfrac{A_{\gamma\pi}}{1-iq_\pi A_{\pi\pi}} \\[2ex] \dfrac{A_{\pi\gamma}}{1-iq_\pi A_{\pi\pi}} & T_{\gamma\gamma} \end{pmatrix},$$

(10)

where

$$A_{\gamma\pi} = A_{\pi\gamma} = K_{\gamma\pi}/(1-iq_\gamma K_{\gamma\gamma}),$$

$$A_{\pi\pi} = K_{\pi\pi} + i K_{\gamma\pi}^2 q_\gamma/(1-iq_\gamma K_{\gamma\gamma}).$$

As before, we are not interested in $T_{\gamma\gamma}$. The forms of $K_{\eta\eta} = K_{\eta\eta}(a)$, $K_{\pi\eta}$, K_{33}, $K_{\pi 3}$, and $K_{\eta 3}$ are the same as given above. However,

$$K_{\pi\pi} \to K_{\pi\pi}(b) = K_{\pi\pi}(a) + i\frac{K_{\pi\eta}q_\eta K_{\eta\pi}}{1-iq_\eta K_{\eta\eta}(a)}. \quad (11)$$

Also we now need

$$K_{\gamma\pi} = B_{\gamma\pi} + \frac{\sqrt{\gamma_\gamma(0)\gamma_\pi(0)}}{E_0 - E} + \frac{\sqrt{\gamma_\gamma(1)\gamma_\pi(1)}}{E_1 - E}$$

$$+ i\frac{K_{\gamma\eta}q_\eta K_{\eta\pi}}{1-iq_\eta K_{\eta\eta}(a)} + i\frac{K_{\gamma3}q_3 K_{3\pi}}{1-iq_3 K_{33}}, \quad (12)$$

$$K_{\gamma\gamma} = \frac{\gamma_\gamma(0)}{E_0 - E} + \frac{\gamma_\gamma(1)}{E_1 - E} + i\frac{K_{\gamma\eta}q_\eta K_{\eta\gamma}}{1-iq_\eta K_{\eta\eta}(a)} + i\frac{K_{\gamma3}q_3 K_{3\gamma}}{1-iq_3 K_{33}}, \quad (13)$$

where the last terms on the rhs represent the effect of the eliminated ηN and $\pi\pi N$ channels. Also we need

$$K_{\gamma\eta} = B_{\gamma\eta} + \frac{\sqrt{\gamma_\gamma(0)\gamma_\eta(0)}}{E_0 - E} + i\frac{K_{\gamma3}q_3 K_{3\eta}}{1-iq_3 K_{33}}. \quad (14)$$

The definitions of all other parameters are the same as for $T_{1,2}$.

III. FITTING STRATEGY AND RESULTS

Compared with Ref. [12] there are now four new parameters $B_{\gamma\pi}$, $B_{\gamma\eta}$, $\gamma_\gamma(0)$, and $\gamma_\gamma(1)$ explicitly dependent on the index γ. These four parameters replace the single free parameter $A(\text{Phot})$ that related $\sigma(\gamma N \to \eta N)$ and $T_{\eta\eta}$. In all there are now 13 parameters that are determined by a MINUIT fit of up to 158 pieces of data — 23 are πN amplitudes (real and imaginary) [14], 11 are $\pi N \to \eta N$ cross sections [$\sigma(\pi\eta)$] [15], and 53 are $\gamma N \to \eta N$ cross sections [$\sigma(\gamma\eta)$] [1]. In addition, from Ref. [16] we use up to 48 $S11(\gamma N \to \pi N)$ amplitudes in the energy range $1350 \leqslant E_{\text{c.m.}} \leqslant 1650$ MeV. There are several reasons for choosing this upper limit:

(a) We wish to include the full effect of the $N(1535)$.

(b) The $\gamma N \to \pi N$ and $\gamma N \to \eta N$ reactions are closely related and so attempting to fit them simultaneously over very different energy ranges could give misleading results. Therefore, we do not attempt to use the available data at higher energies.

(c) The values of the $\gamma N \to \pi N$ amplitudes are far from being unique — as is clear when comparing the amplitudes of Refs. [16] and [17]. In fact, in view of this lack of uniqueness we do not use the quoted errors of Ref. [16]. Instead, we make two overall fits where, in the one case, all the errors in Ref. [16] are increased to $\pm\sqrt{2}$ for both the real and imaginary components and, in the second case, the increase is only to $\pm 1/\sqrt{2}$. These choices were made so that the resultant χ^2/dpt (data point) for this reaction are comparable to those in the other reactions. We realize that this procedure is throwing away information. However, the main aim in this work is to study the $\gamma N \to \eta N$ reaction with the $\gamma N \to \pi N$ playing only a secondary role as a possible stabilizing effect. Therefore, we want a K-matrix fit that is good for the well established reactions but, at the same time, also reproduces the qualitative trends in the $\gamma N \to \pi N$ reaction suggested by Refs. [16] and [17]. In fact, we could even turn the argument around and say that our $S11$ amplitudes are a *prediction* that is consistent with the other reactions.

In practice, the actual η-production cross-section data was used in a reduced form, from which threshold factors have been removed, namely,

$$\sigma(\pi\eta)_r = \sigma(\pi\eta)\frac{q_\pi}{q_\eta} = \frac{8\pi q_\pi}{3q_\eta}|T_{\pi\eta}|^2$$

and $\quad \tau(\gamma\eta)_r = \sqrt{\sigma(\gamma\eta)\frac{E_\gamma}{4\pi q_\eta}} = |T_{\gamma\eta}|. \quad (15)$

In Ref. [12] the last equation was replaced by $\tau(\gamma\eta)_r = A(\text{Phot})|T_{\eta\eta}|$, where $A(\text{Phot})$ was treated as a free parameter in the MINUIT minimization.

At first, because of the lack of uniqueness in the two analyses published in Refs. [16] and [17], only the 32 $S11(\gamma N \to \pi N)$ amplitudes with $E_{\text{c.m.}} \leqslant 1550$ MeV were used, since this upper energy limit is about the same as for the $\gamma N \to \eta N$ data. This resulted in a good fit with parameters qualitatively the same as in Ref. [12] and also in line with the Particle Data Group [18] — see columns A, D, and PDG in Table I. In column A, the error bars in the $S11(\gamma N \to \pi N)$ amplitudes of Ref. [16] have all been increased to $\pm\sqrt{2}$ — for the reasons discussed earlier. In this case, the overall χ^2/dof and the separate χ^2/dpt are all near unity. However, when in column D the errors are increased to only $\pm 1/\sqrt{2}$, the χ^2/dpt for the $S11(\gamma N \to \pi N)$ amplitudes become significantly larger. Columns B and C show the corresponding results when the $S11(\gamma N \to \pi N)$ data base is increased to include data with $E_{\text{c.m.}}$ up to 1650 MeV. The fits are now systematically worse than in column A with the overall χ^2/dof increasing from 0.89 to 1.23 in column B. In column C — the case with smaller errors and the larger data base — the fit obtained was quite poor to such an extent that reasonable errors on the parameters could not be extracted. The latter fit, when all 13 parameters were varied simultaneously, did not give from MINUIT a Migrad result that converged to sensible parameters. The fit displayed in column C is based on the parameters of column B, some of which are first fixed and then released and scanned by MINUIT. The

TABLE I. The optimized parameters from MINUIT defining the K matrices: There are in column A only 32 $\gamma N \rightarrow \pi N$ data points with $E_{c.m.} \leqslant 1550$ MeV and error bars all 1.41, in column B 48 data points with $E_{c.m.} \leqslant 1650$ MeV and error bars all 1.41. Cases D and C are the same as A and B except that the error bars are reduced to 0.70. In addition, the first column shows the results from Ref. [12] and the last column the corresponding values from the Particle Data Group [18].

	[12]	A	D	B	C	(PDG) [18]
$B_{\eta\eta}$(fm)	0.177(33)	0.263(32)	0.228(106)	0.371(48)	0.372	–
$B_{\pi\eta}$(fm)	0.022(13)	0.016(8)	0.027(17)	0.003(15)	0.019	–
E_0(MeV)	1541.0(1.6)	1536.8(0.9)	1540.6(6.6)	1530.0(2.5)	1529.5	1535(20)
E_1(MeV)	1681.6(1.6)	1682.1(1.6)	1683.2(1.6)	1682.9(1.6)	1685.4	1650(30)
$\Gamma(Total)$(MeV)	148.2(8.1)	138.2(1.3)	142.7(13.4)	122.4(5.0)	114.4	100–250
η(br)	0.568(11)	0.585(8)	0.594(18)	0.61(17)	0.648	0.30–0.55
π(br)	0.394(9)	0.380(6)	0.371(13)	0.358(8)	0.330	0.35–0.55
$\Gamma(Total,1)$(MeV)	167.9(9.4)	171.7(6.3)	183.8(9.2)	178.8(7.8)	203.8	145–190
π(br,1)	0.735(11)	0.729(10)	0.721(11)	0.724(10)	0.709	0.55–0.90
A(Phot)	19.74(36)					
$B_{\gamma\eta}$(fm)		0.0040(1)	0.0049(15)	0.0027(9)	0.0036	
$B_{\gamma\pi}$(fm)		0.0030(4)	0.0034(5)	0.0013(7)	0.0021	
$\gamma_\gamma(0)$		0.00018(1)	0.00018(2)	0.00016(1)	0.00014	
$\gamma_\gamma(1)$		$\leqslant 10^{-8}$	$\leqslant 10^{-8}$	$7(2)10^{-5}$	$6(1)10^{-5}$	
$\chi^2(\gamma N \rightarrow \eta N)$/dpt	0.75	0.75	0.75	0.79	0.94	
$\chi^2(\pi N \rightarrow \eta N)$/dpt	0.73	0.69	0.67	0.93	2.10	
$\chi^2(\pi N \rightarrow \pi N)$/dpt $\mathcal{R}$	0.94	1.04	1.52	1.27	2.89	
$\chi^2(\pi N \rightarrow \pi N)$/dpt $\mathcal{I}$	0.60	0.56	0.63	0.48	0.92	
$\chi^2(\gamma N \rightarrow \pi N)$/dpt $\mathcal{R}$		0.59	2.09	1.34	3.83	
$\chi^2(\gamma N \rightarrow \pi N)$/dpt $\mathcal{I}$		1.33	4.27	2.25	5.53	
χ^2(Total)/dof	0.83	0.89	1.54	1.23	2.66	

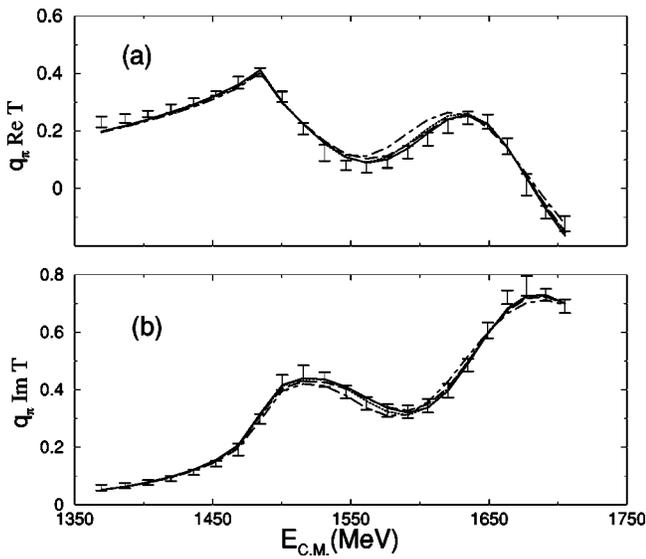

FIG. 1. The (a) real and (b) imaginary parts of the s-wave $\pi N \rightarrow \pi N$ amplitudes of Ref. [14]. Solid line for solution A, dashed for D, dotted for B, and dash-dot for C.
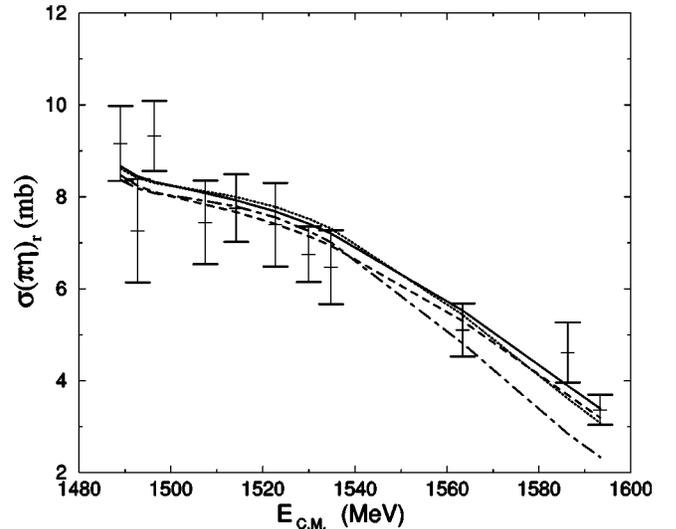
FIG. 2. The $\pi N \rightarrow \eta N$ reaction. Data is from Ref. [15]. Notation as in Fig. 1.
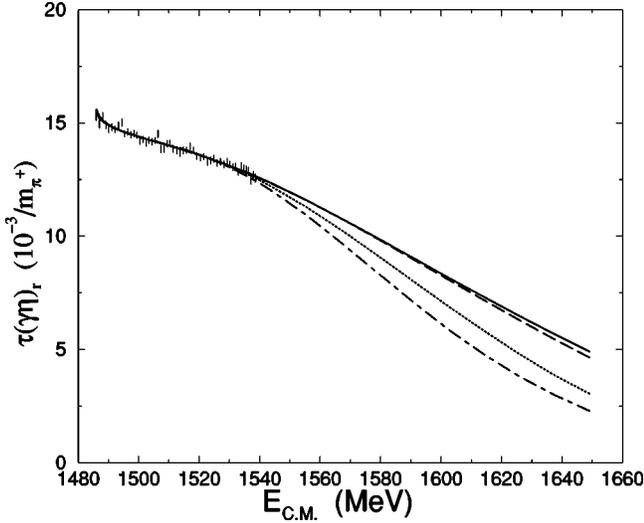
FIG. 3. The $\gamma N \to \eta N$ reaction. Data is from Ref. [1]. Notation as in Fig. 1.

comparison with the data being fitted is shown in Figs. 1–4. The main conclusions to be drawn from Table I and these figures are: (1) All four fits to the data are reasonable with cases A and B being superior. (2) The main distinguishing feature between the four fits is the relative ability to fit the $S11(\gamma N \to \pi N)$ data, since this is the channel that contributes most to the overall χ^2/dof — with the χ^2/dpt's from the other four channels being reasonably constant and comparable to unity in all fits. This suggests that it will be hard for the present type of analysis to maintain these latter χ^2/dpt's and, at the same time, achieve a good χ^2/dpt for the $S11(\gamma N \to \pi N)$ data presented in Refs. [16] and [17]. The authors, therefore, suggest that the $S11(\gamma N \to \pi N)$ amplitudes from the K-matrix model could be a more realistic set
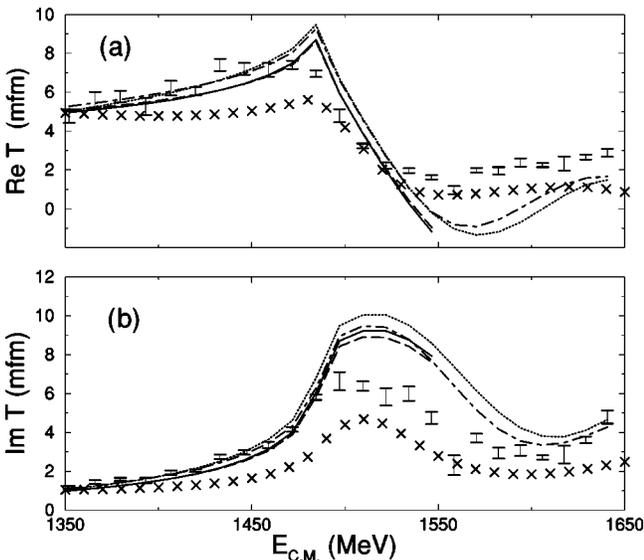

FIG. 4. The (a) real and (b) imaginary parts of the $S11\gamma N \to \pi N$ of Ref. [16]. Crosses are data from Ref. [17]. Notation as in Fig. 1.

TABLE II. Conversion from the parameters $\Gamma(\text{Total})$, $\eta(\text{br})$, $\pi(\text{br})$, $\Gamma(\text{Total},1)$, $\pi(\text{br},1)$ in Table I and to the parameters $\gamma_\eta(0)$, $\gamma_\pi(0, 1)$, and $\gamma_3(0, 1)$ used in the formalism. The conversion $\gamma_\gamma(0,1)$ to $\Gamma_\gamma(0,1)$ and the 2-π branching ratio(2-π br) are also given. The other notations are the same as Table I.

	[12]	A	D	B	C
$\gamma_\eta(0)$	0.226	0.217	0.227	0.202	0.199
$\gamma_\pi(0)$	0.063	0.056	0.057	0.047	0.040
$\gamma_\pi(1)$	0.113	0.115	0.121	0.118	0.132
2-π br	0.038	0.035	0.035	0.027	0.022
$\gamma_3(0)$	0.0134	0.0114	0.0120	0.0079	0.0059
$\gamma_3(1)$	0.0906	0.0945	0.1043	0.1004	0.1208
$\Gamma_\gamma(0)(\text{MeV})$		0.171	0.172	0.157	0.136
$\Gamma_\gamma(1)(\text{MeV})$		0	0	0.080	0.068

than those in Refs. [16] and [17], since they are now consistent with more reactions $\pi N \to \pi N$, $\pi N \to \eta N$ and $\gamma N \to \eta N$. (3) Figure 3 shows that, beyond $E_{\text{c.m.}} \approx 1550$ MeV, cases A and D give larger cross sections than B and C — the difference increasing to about a factor of 2 by $E_{\text{c.m.}} \approx 1650$ MeV. In the near future, the GRAAL Collaboration [2] is expected to provide total cross-section data up to this energy and so, hopefully, distinguish between these cases.

In Table I the parameters $\Gamma(\text{Total})$, $\eta(br)$, $\pi(br)$, $\Gamma(\text{Total},1)$, and $\pi(br,1)$ are quoted, whereas the earlier formalism is expressed in terms of $\gamma_\eta(0)$, $\gamma_\pi(0, 1)$, and $\gamma_3(0, 1)$. The two notations are related as follows:

  (1) $\gamma_\eta(0) = 0.5\Gamma(\text{Total}) \eta(\text{br})/q_\eta[E_0(R)]$,
  (2) $\gamma_\pi(0) = 0.5\Gamma(\text{Total}) \pi(\text{br})/q_\pi[E_0(R)]$,
  (3) $\gamma_\pi(1) = 0.5\Gamma(\text{Total}, 1) \pi(\text{br}, 1)/q_\pi[E_1(R)]$,
  (4) $\gamma_3(0) = 0.5\Gamma(\text{Total})[1 - \eta(\text{br}) - \pi(br)]/q_3[E_0(R)]$,
  (5) $\gamma_3(1) = 0.5\Gamma(\text{Total}, 1)[1 - \pi(\text{br}, 1)]/q_3[E_1(R)]$,
and (6) $\Gamma_\gamma(0,1) = 2q_\gamma[E_{0,1}(R)]\gamma_\gamma(0,1)$.

This now requires a choice to be made for the reference energies $E_0(R)$ and $E_1(R)$, which preferably should be close to the $E_{0,1}$ in Table I. Here, we take simply $E_{0,1}(R) = 1535$, 1650 MeV, respectively. This gives $q_\eta[E_0(R)] = 0.945$, $q_\pi[E_0(R)] = 2.365$, $q_\pi[E_1(R)] = 2.770$, $q_3[E_0(R)] = 1.067$, $q_3[E_1(R)] = 1.245$, $q_\gamma[E_0(R)] = 2.436$, and $q_\gamma[E_1(R)] = 2.829$ fm^{-1}. It should be added that this is not an assumption or an approximation. It is just setting a scale that is needed when converting from one notation to the other. In Table II, the $\gamma_{\pi,\eta,3}(0,1)$ are tabulated along with $\Gamma_\gamma(0,1)$.

In the above, we have been very explicit in describing the formalism. Therefore, in principle, the reader should be able to reconstruct all three T matrices and so determine each of the complex amplitudes needed in the five processes $\pi N \to \pi N$, $\pi N \to \eta N$, $\eta N \to \eta N$, $\gamma N \to \pi N$, and $\gamma N \to \eta N$. This formalism also enables these amplitudes to be calculated at unphysical energies. For example, in the study of possible η-nucleus quasibound states, the $\eta N \to \eta N$ amplitudes are needed below the η threshold. This is easily achieved by simply using an η momentum(q_η) that is purely imaginary.

TABLE III. Results for the scattering length (a), effective range (r_0), and Shape parameter (s) compared with earlier works. The other notations are the same as Table I.

	[12]	A	D	B	C
a in fm	$0.75(4)+i0.27(3)$	$0.87+i0.27$	$0.83+i0.27$	$1.05+i0.27$	$1.07+i0.26$
r_0 in fm	$-1.50(13)-i0.24(4)$	$-1.31-i0.28$	$-1.34-i0.22$	$-1.19-i0.31$	$-1.25-i0.25$
s in fm^3	$-0.10(2)-i0.01(1)$	$-0.14-i0.03$	$-0.12-i0.01$	$-0.18-i0.06$	$-0.20-i0.05$

In spite of the model being very explicit, it is sometimes convenient to have simplified versions of some of the amplitudes. The ones we consider are those that are expansions in terms of q_η about the η threshold, in particular $A_{\eta\eta}$ and $A_{\gamma\eta}$. The former results in the usual $\eta N \rightarrow \eta N$ effective range expansion of Ref. [12], the parameters of which are now updated in Table III. This shows that the scattering length(a) is larger than that extracted in Ref. [12] — the increase being 15% for case A and 40% for case B. However, it should be remembered that case B extrapolates the model into a region where the $\gamma N \rightarrow \eta N$ data is lacking, and it is just this reaction that is crucial in determining the scattering length. Given this expansion, then $T_{\eta\eta}$ is readily calculated from $A_{\eta\eta}$ as in Eq. (1) at energies both above and below the η threshold. The other amplitude of interest is $T_{\gamma\eta}$ in Eq. (4), which is seen to depend on both $A_{\eta\eta}$ and $A_{\gamma\eta}$. By analogy with the expansion of $T_{\eta\eta}$, we express $T_{\gamma\eta}$ in the form

$$\frac{1}{T_{\gamma\eta}} = \frac{1}{A_{\gamma\eta}} - iq_\eta \frac{A_{\eta\eta}}{A_{\gamma\eta}}. \qquad (16)$$

The two entities $1/A_{\gamma\eta}$ and $A_{\eta\eta}/A_{\gamma\eta}$ are then expanded as $e_i + f_i q_\eta^2 + g_i q_\eta^4$ with the parameters e_i, f_i, g_i being given in Table IV. Both of these expansions do very well over the energy range of Ref. [1]. For example, with case A at $E_{\text{c.m.}} = 1538.6$ MeV, an energy that is 50 MeV above the η threshold, the expansion of $1/A_{\gamma\eta}$ gives $8.4-i20.0$ fm^{-1} compared with the exact value of $7.9-i19.7$ fm^{-1} and the expansion of $A_{\eta\eta}/A_{\gamma\eta}$ gives $37.12-i5.4$ compared with the exact value of $37.08-i5.7$. This latter agreement and the weak energy dependence of this quantity explains why, in Ref. [12], the replacement of $\sigma(\gamma N \rightarrow \eta N) \propto |T_{\gamma\eta}|^2$ by

$\sigma(\gamma N \rightarrow \eta N) \propto |T_{\eta\eta}|^2$ was a good approximation, since, as seen from Eqs. (1) and (4), $T_{\gamma\eta} = A_{\gamma\eta} T_{\eta\eta}/A_{\eta\eta} \rightarrow A(\text{Phot})T_{\eta\eta}$. Also the value of $A(\text{Phot}) = 19.74(36)$ in Table I is essentially given by $1/e_2 \approx \frac{1}{40} m_\pi \ 10^3 \approx 18$. In Fig. 5, the real and imaginary components of $T_{\gamma\eta}$ are shown, when these two expansions are used in Eq. (16), which is then inverted to give $T_{\gamma\eta}$. It is seen that they give a good representation over a wide energy range especially for energies below the η threshold. This agreement is very similar to that found in Ref. [12] for $T_{\eta\eta}$. It should be added that, if the form of $T_{\gamma\eta}$ written in Eq. (4) is used directly with expansions of $A_{\gamma\eta}$ and $A_{\eta\eta}$, then the fit is much poorer, as also seen in Fig. 5.

IV. DISCUSSION AND CONCLUSIONS

In this paper the authors have developed a simple K-matrix parametrization that gives, in an energy range of about 100 MeV each side of the η threshold, a good fit to $\pi N \rightarrow \pi N$, $\pi N \rightarrow \eta N$, and $\gamma N \rightarrow \eta N$ data. In addition, it has the same trends as the $\gamma N \rightarrow \pi N$ data, which at present is not unique over this energy range. However, this consistent fit should not be considered an end in itself, since it also results in predictions for the $\eta N \rightarrow \eta N$ S-wave amplitude. Near the η threshold this amplitude has been parametrized in the form of the effective range expansion — the resultant parameters being given in Table III. Since this expansion is good over a wide energy range each side of the η threshold, it is very useful for discussions concerning the possibility of η-nucleus quasibound states, e.g., in Ref. [19] the effective range expansion of Ref. [12] was used to study the production of η nuclei, while Ref. [20] uses such an expansion to describe η-nucleus final-state interactions. The indications

TABLE IV. The parameters e_i, f_i, g_i in the expansions $e_i + f_i q_\eta^2 + g_i q_\eta^4$ for $1/A_{\gamma\eta}(i=1)$ and $A_{\eta\eta}/A_{\gamma\eta}(i=2)$. The other notations are the same as Table I.

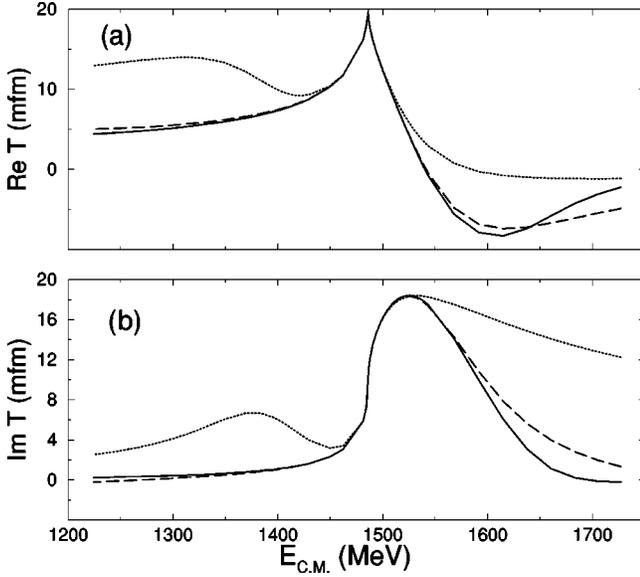| For $1/A_{\gamma\eta}$	A	D	B	C
e_1 in fm^{-1}	$40.7-i18.6$	$40.9-i18.0$	$39.9-i20.5$	$40.6-i19.3$
f_1 in fm	$-31.0-i2.0$	$-27.7-i1.9$	$-39.4-i0.4$	$-39.1+i0.2$
g_1 in fm^3	$-3.9+i0.6$	$-4.1+i0.6$	$-4.1+i2.0$	$-6.2+i2.2$
For $A_{\eta\eta}/A_{\gamma\eta}$				
e_2	$40.6-i5.2$	$38.6-i4.0$	$47.4-i10.9$	$48.4-i10.2$
f_2 in fm^2	$-3.4-i0.7$	$-1.1-i0.5$	$-10.1-i2.1$	$-8.2-i2.0$
g_2 in fm^4	$-0.4+i0.1$	$-0.1+i0.1$	$-0.8+i0.1$	$-1.1+i0.1$

FIG. 5. The (a) real and (b) imaginary parts of $T_{\gamma\eta}$. The solid curve is the exact value as given by the model. The dashed curve uses expansions of $1/A_{\gamma\eta}$ and $A_{\eta\eta}/A_{\gamma\eta}$, whereas the dotted curve uses those for $A_{\gamma\eta}$ and $A_{\eta\eta}$.

from Table III are that the $\eta-N$ scattering length is now larger than that extracted in Ref. [12]. This is even more favorable for the existence of η-nucleus quasibound states and may lead to an early onset of nuclear P-wave states, which are easier to detect in the Darmstadt experiment outlined in Ref. [21].

One result of the above fits is the extraction of the photon-nucleon-$N(1535)$ coupling constant $\gamma_\gamma(0,1)$ as indicated in Table I, which is equivalent to the partial decay width Γ_γ for $N(1535)\rightarrow\gamma N$. The definition of Γ_γ is not unique, however. Below, this question is elucidated on a simple soluble model of the T matrix. This model is also used to understand the interference of a resonant interaction described by a singularity in the K matrix and potential interactions described by the background parameters B.

Let us, assume a separable K-matrix model with

$$K_{i,j}=\sqrt{\gamma_i\gamma_j}\left(\frac{1}{E_0-E}+B\right), \quad (17)$$

where, in the notation of Eqs. (3) and (6), $B_{ij}=B\sqrt{\gamma_i\gamma_j}$. This leads to a separable solution for the T matrix

$$T_{i,j}=\sqrt{\gamma_i\gamma_j}\ \frac{1+B(E_0-E)}{E_0-E-i\sum_k q_k\gamma_k[1+B(E_0-E)]}. \quad (18)$$

When the background term B vanishes, this model is equivalent to simple Breit-Wigner multichannel resonances of eigenwidth $\Gamma/2=\Sigma_k q_k\gamma_k$. However, when we relax this restriction a new structure is built upon the resonance. It is

determined by the energy-dependent term $[1+B(E_0-E)]$, which generates a zero of the cross section at $E=E_0+1/B$. Now, it is the $1/B$ that sets a new energy scale, which may be independent of the scale given by the width. For a large B one finds the resonance to be accompanied by a nearby zero, whereas for small B this zero is moved away beyond the resonance width. The resonance shape is thus very different from the Lorentian : one reason being the strong energy dependence in $q_k(E)$ and another being the pole-background interference.

As discussed above in connection with Table II, it is usually natural to define the partial width of a resonance on the basis of Eqs. (17) and (18) as $\Gamma_\gamma(0,1)=2q_\gamma(E_{0,1})\gamma_\gamma(0,1)$. For the best fits to the data (sets A, B of Table I), this equation produces $\Gamma_\gamma(0)=0.171$, 0.157 MeV, and $\Gamma_\gamma(1)=0.0$, 0.080 MeV, respectively. However, with complicated phenomenological T matrices one could define Γ_γ otherwise, e.g., by moulding T into the Breit-Wigner form in the proximity of $E=E_0$. Thus, at $\text{Re}\,T_{\gamma,j}=0$ one has

$$\text{Im}\,T_{\gamma,j}=\frac{\sqrt{(\Gamma_\gamma/q_\gamma)(\Gamma_j/q_j)}}{\Gamma}=\frac{\sqrt{(\Gamma_\gamma/2q_\gamma)\gamma_j}}{\Gamma/2}.$$

Inserting from Table II the values of Γ and γ_j gives another estimate of Γ_γ. For example, with case A, $\text{Re}\,T_{\gamma,\eta}=0$ at $E=1540$ MeV giving $\text{Im}\,T_{\gamma,\eta}=0.0179$ and $q_\gamma=2.45$ fm^{-1}. This results in $\Gamma_\gamma=0.176$ MeV. Similarly, $\text{Re}\,T_{\gamma,\pi}=0$ at $E=1535$ MeV giving $\text{Im}\,T_{\gamma,\pi}=0.0085$ and $q_\gamma=2.43$ fm^{-1}. This results in $\Gamma_\gamma=0.150$ MeV. The proximity of these three widths reflects the fact that the realistic situation is fairly close to the separability situation described by Eqs. (17) and (18). It is found to hold approximately, for all the parameter sets in Table I.

There is another, somewhat unexpected effect of the $[1+B(E_0-E)]$ interference term in Eq. (18). For $B>0$ one finds that the amplitudes below the resonance are enhanced, and the amplitudes above the resonance are reduced with respect to the pure resonance term. This effect is seen clearly for the B and C parameter sets, where below the resonance the $B_{\eta\eta}$ parameter in the $\eta-N$ channel is the largest and the real parts of the $\eta-N$ scattering lengths given in Table III are also the largest. On the other hand, the (γ,η) production cross section, dominated by the final-state $\eta-N$ interactions, become the smallest above the resonance as seen Fig. 4. One consequence of this effect is that an extension of the (γ,η) cross-section measurements to energies above the $N(1535)$ resonance may by instrumental in fixing more precisely the $\eta-N$ scattering length. As indicated in the introduction, the real part of this scattering length is crucial in the determination of quasibound states in η-few nucleon systems.

On the experimental side there are several groups [1,2] studying the $\gamma N\rightarrow\eta N$ reaction in or near this interesting energy range. The observation of the cross section near and above $E_{\text{c.m.}}=1540$ MeV would be of great interest, enabling a detailed study to be made of the $N(1535)$ and possibly leading to a better understanding of the internal structure of this object. At present there is no definite conclusion as to whether or not this resonance structure is due to a pole in the

K matrix, as advocated here, or arising through coupling to high-lying closed channels — see Ref. [22].

In the near future, the authors of Ref. [16] are expected to extract, directly from experiment, separate values for the real and imaginary components of $T(\gamma\eta)$. These will be analogous to the $S11\gamma N \rightarrow \pi N$ data already available in Ref. [16] and used in the above fits. Such a development will then enable the present type of K-matrix analysis to be even more constrained.

[1] B. Krusche *et al.*, Phys. Rev. Lett. **74**, 3736 (1995); M. Fuchs *et al.*, Phys. Lett. B **368**, 20 (1996).

[2] J. Ajaka *et al.*, Phys. Rev. Lett. **81**, 1797 (1998).

[3] E. Chiavassa *et al.*, Phys. Lett. B **337**, 192 (1994).

[4] H. Calén *et al.*, Phys. Lett. B **366**, 39 (1996); A.M. Bergdolt *et al.*, Phys. Rev. D **48**, R2969 (1993).

[5] J.T. Balewski *et al.*, Acta Phys. Pol. B **27**, 2911 (1996).

[6] R.S. Bhalerao and L.C. Liu, Phys. Rev. Lett. **54**, 865 (1985).

[7] Q. Haider and L.C. Liu, Phys. Lett. B **172**, 257 (1986); Phys. Rev. C **34**, 1845 (1986).

[8] Ch. Sauerman, B.L. Friman, and W. Nörenberg, Phys. Lett. B **341**, 261 (1995).

[9] C. Bennhold and H. Tanabe, Nucl. Phys. **A530**, 625 (1991).

[10] N. Kaiser, P.B. Siegel, and W. Weise, Nucl. Phys. **A594**, 325 (1995).

[11] M. Arima, K. Shimizu, and K. Yazaki, Nucl. Phys. **A543**, 613 (1992).

[12] A. M. Green and S. Wycech, Phys. Rev. C **55**, R2167 (1997).

[13] M.L. Goldberger and K.M. Watson, *Collision Theory* (Wiley, New York, London, 1964).

[14] R. Arndt, J.M. Ford, and L.D. Roper, Phys. Rev. D **32**, 1085 (1985). Solution SM95 obtained from SAID via Internet in November 1996.

[15] M. Clajus and B.M.K. Nefkens, π-N Newsletter **7**, 76 (1992).

[16] R.A. Arndt, I. Strakovski, and R.L. Workman, Phys. Rev. C **53**, 430 (1996); http://said.phys.vt.edu/.

[17] D. Drechsel, O. Hanstein, S.S. Kamalov, and L. Tiator, Nucl. Phys. **A645**, 145 (1999).

[18] Particle Data Group, Eur. Phys. J. C **3**, 1 (1998).

[19] A.I. Lv́ov, Proceedings of the International Conference on Mesons and Nuclei, Prudhonice, Prague, 1998, edited by J. Adams (World Scientific, Singapore, in press), nucl-th/9809054; G.A. Sokol *et al.*, ''Search for η-mesic nuclei in photomesonic processes,'' nucl-ex/9812007.

[20] M. Effenberger and A. Sibirtsev, Nucl. Phys. **A632**, 99 (1998).

[21] R.S. Hayano, S. Hirenzaki, and A. Gillitzer, ''Formation of η-mesic Nuclei Using the Recoilless $(d,{}^{3}\text{He})$ Reaction,'' nucl-th/9806012.

[22] R. A. Arndt, A.M. Green, R.L. Workman, and S. Wycech, Phys. Rev. C **58**, 3636 (1998).